COVER SHEET

Paper Number: 510

Title: *A Technique for Mapping Characteristic Lengths to Preserve Energy Dissipated via Strain Softening in a Multiscale Analysis* Proceedings of the **American Society for Composites Twenty-Ninth Technical Conference**

Authors: Evan J. Pineda
Brett A. Bednarcyk
Steven M. Arnold

ABSTRACT

INTRODUCTION

An advantage composites possess over most monolithic materials as a structural engineering material is that, in addition to the physical properties of the constituents, the subscale geometry (architecture) of the constituents contribute to the apparent response of the composite, yielding a material which exhibits behavior that surpasses the sum of its constituents. Often, these details are smeared into a homogenized model for convenience, and ad-hoc assumptions are used to include the effects of the composite micro-architecture, in computational analysis methods. These assumptions work well to predict the elastic behavior of composite materials. However, to incorporate the non-linear effects of damage and failure, increasingly complicated continuum damage theories and failure criteria must be developed. Many, but not all, of these theories incorporate various non-physical parameters that must be calibrated in order to capture the appropriate failure modes in the composite.

The deficiencies of homogenized models become more apparent when strain localization leading to softening damage occurs in the material. Once localization occurs, the characteristic length of the material transitions from a length on the order of hundreds to thousands of repeating unit cells (RUCs) to that on the order of a representative volume element (RVE) composed of enough microstructural elements (grains, inclusions, etc.), such that the RVE behavior

Evan J. Pineda, Aerospace Research Engineer
Brett A. Bednarcyk, Materials Research Engineer
Steven M. Arnold, Technical Lead
Multiscale and Multiphysics Modeling Branch, NASA Glenn Research Center, 21000 Brookpark Rd., Cleveland, OH 44135.

is typical of the bulk composite (with an embedded localization), on average. Typically, an RUC does not have a physical length associated with it, but an RVE must have a physical length associated with it, and the RVE must contain a large enough volume that it captures the essence of the microstructure from a physical standpoint.

Multiscale modeling is a popular technique for incorporating microscale effects into a structural scale model. With these methods, micromechanics models are linked to structural models and localization details, at the microscale, are captured directly during down-scaling, while homogenization is employed for up-scaling, to communicate the effects of localization by smearing over the subscale model. The linking of scales can be achieved in a hierarchical, concurrent, or synergistic sense [1, 2]. With hierarchical multiscale approaches, micromechanics or subscale simulations are preformed *a priori*, and the results obtained from those simulations are utilized in subsequent macroscale, or structural level, models. With concurrent multiscale modeling, both the micro and macro scales operate simultaneously in time and space. Finally, synergistic multiscale models operate concurrently in time and hierarchically in both spatial scales (up-scaling and down-scaling), or vice versa.

Physically, a continuum material must posses a positive-definite tangent stiffness tensor, and, in fact, at a small enough scale, the material tangent stiffness tensor always remains positive-definite in order to satisfy the necessity of having a real, local speed of sound [3]. However for practical purposes, engineers must model structures at scales much larger than the characteristic flaws in the material. The homogenized (over a representative volume whose characteristic length is larger than the typical flaw size) continuum representation of a material containing the nucleation and propagation of discontinuities, such as cracks or voids, will exhibit post-peak strain softening in the macroscopic stress-strain response. Although micromechanics and multiscale methods can be utilized to introduce details of the composite microstructure into structural analyses, erroneous numerical failure predictions can be obtained when post-peak strain softening is exhibited in the material, regardless of the scale. Loss of positive-definiteness of the tangent stiffness tensor leads to a material instability, which manifests as a localization of damage into the smallest length scale in the continuum problem [3]. Since the post-peak stress-strain relationship prescribes the energy density dissipated during the failure process, the total amount of energy dissipated is proportional to the size of the localization element, and in the limit as the element size is decreased, zero energy is required to fail the structure [4, 5]. Thus, the computational results will become pathologically dependent on the mesh size.

A simple way to overcome this deficiency is to judiciously scale the post-peak softening slope by the characteristic element length such that the total energy release rate in the post-peak regime, after reaching a state of zero stress, is equal to the critical energy release rate, or fracture toughness, of the material (a fixed, experimentally obtained material parameter). This approach, known as the crack band or smeared crack approach, has been used by many authors

to model strain localization due to failure within an FEM framework in a mesh objective manner [6, 7, 8, 3].

Previously the authors[9] implemented the crack band model[6] within the generalized method of cells (GMC)[10] and high-fidelity generalized method of cells (HFGMC)[11] micromechanics theories and the predictions were verified against analogous FEM models. Non-local, or gradient-based theories have also been shown to prevent strain localization, eliminating dependence of the numerical solution on the size of the elements, as discussed in, [12, 13, 14]. However, the latter techniques require higher-order numerical interpolations and can be challenging to implement.

Once a mesh objective theory has been implemented in a single scale analysis, the energy dissipation is preserved regardless of the size of the mesh, at that scale. However in a multiscale analysis, careful attention must be paid to how energy is being preserved and transferred across the various length scales[15]. However, if the appropriate theories are in employed at the correct scales and a consistent "handshaking" methodology is used that yields an appropriate localization limiter at the macroscale, then both the energy density and energy release rate will be preserved across the scales.

In previous work, the dimensions of the microscale RUC were scaled directly by the characteristic length of the element [16]. Objectivity was shown for square elements, however, the energy is not preserved identically across the scales if the macroscale finite element is irregularly shaped or has an aspect ratio other than one. In this, work a transformation is used to map the characteristic lengths within the RUC directly to the macroscale element domain. These mapped lengths are used in the local crack band calculations to regularize the energy dissipation. The results of multiscale simulations with various, macroscale, finite element meshes (containing elements with different aspect ratios) are compared utilizing the novel mapping technique, the direct scaling method, and fixed (independent of element size) RUC dimensions.

MULTISCALE MODELING OF COMPOSITE STRUCTURES USING GMC

In GMC, a doubly-periodic RUC is represented with N_β x N_γ subcells. A GMC representation of a unidirectional, fiber-reinforced composite containing square-packed fibers is shown in Figure 1. Although a 2D representation is shown, the calculated, local fields in the RUC are fully 3D, but there is no variation in the fields along the x_1-direction. Subcells in the RUC are identified by the indices β (in the x_2-direction) and γ (in the x_3-direction), and the RUC dimensions are given by H and L.

RUCs modeled with GMC can be easily linked to higher-level, structural FEM models. The integration point strains, from the FEM model, are applied to the RUC and the local subcell fields are determined using GMC; this process is referred to herein as down-scaling for clarity, although in literature it is more

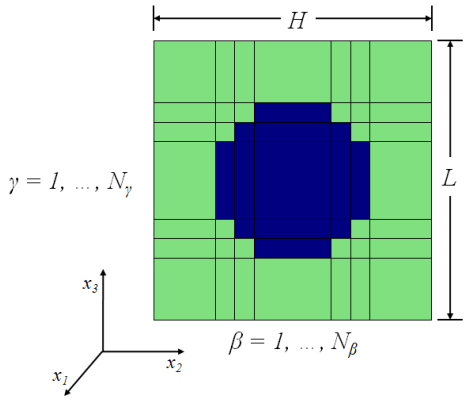

Figure 1. Doubly-periodic representation of a unidirectional, fiber-reinforced composite containing square-packed fibers using GMC.

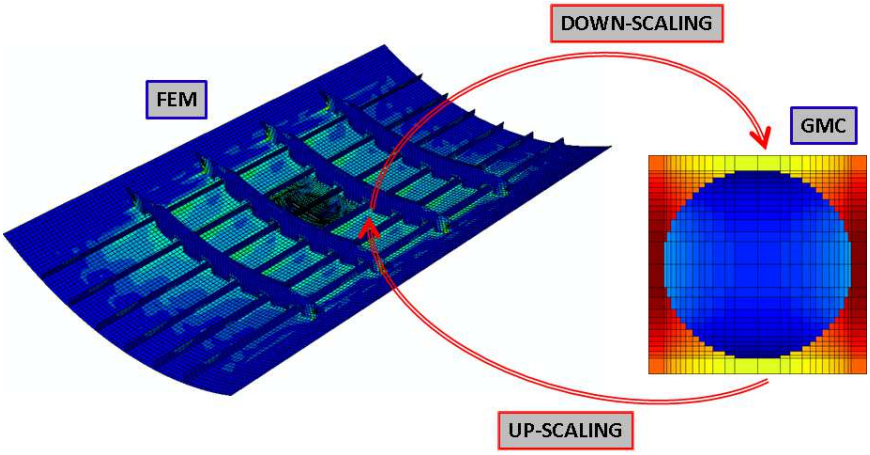

Figure 2. Schematic representation of the up-scaling and down-scaling steps employed in the synergistic multiscale technique utilizing GMC and FEM.

often referred to as localization. If the subcell material behavior is nonlinear, the local stresses and strains are used to calculate the local stiffnesses, inelastic strains, thermal strains, and/or state variables. Since the local stresses and strains depend on the local stiffnesses, inelastic strains, and thermal strains, some iterations of this procedure may be necessary to resolve the correct local fields if there is a high degree of nonlinearity. The RUC is then homogenized and the global stiffnesses, inelastic strains, thermal strains, and/or state variables are computed and passed onto the macroscale in a process referred to as up-scaling. The global stresses and material Jacobian at the integration point are then computed using the up-scaled, global, homogenized fields. A schematic showing this procedure and the corresponding scales is presented in Figure 2.

Preserving Energy Across Scales Using Consistent 'Hand-shaking' Methods

The lack of positive definiteness of the elastic, or inelastic, tangent stiffness tensor leads to imaginary wave speeds in the material. The longitudinal wave speed in an isotropic material is given by

$$c_L = \sqrt{\frac{E(1-\nu)}{\rho(1+\nu)(1-2\nu)}} \tag{1}$$

where c_L is the wave velocity, E is the Young's modulus of the material, ν is the Poisson's ratio, and ρ is the material density. A one-dimensional approximation yields $v = \sqrt{\frac{E}{\rho}}$. The existence of an imaginary wave speed results in a boundary value problem that is ill-posed [4, 5, 17, 3]. Physically, a material must possess a positive-definite tangent stiffness tensor, and in fact, at the micro-scale the material tangent stiffness tensor always remains positive-definite. However for practical purposes, engineers must model structures at scales much larger than the flaws in the material, and the homogenized continuum representation of a material with nucleation and propagation of discontinuities, such as cracks or voids, exhibits post-peak strain softening in the macroscopic, homogenized, stress-strain response. This homogenized response is assumed to govern over a suitable volume of the material, appropriate to the microstructure of the material.

Loss of positive-definiteness of the tangent stiffness tensor leads to a material instability which manifests as a localization of damage into the smallest length scale in the continuum problem; in a discretized, numerical setting this is a single discretization element [3]. For simplicity, FEM is considered the numerical framework for this discussion and the discretization element is a finite element. However, the same localization and discretization-based dependence applies to GMC, where the damage localizes to a subcell. Thus in a numerical setting, the post-peak softening strain energy is dissipated over the volume of the element to which the damage localizes. Since a stress-strain relationship prescribes the energy density (energy per unit volume) dissipated during the failure process, the total amount of energy dissipated in the element decreases as the size of the element is reduced. Figure 3 illustrates the load-displacement response of a discretized, tensile bar as the size of the elements is reduced (i.e., as the mesh is refined). For a given element size, the load-displacement response exhibits non-physical snap back, and in the limit as the element size approaches zero, the amount of energy dissipated during the failure also approaches zero.

With the crack band model, the post-peak tangent slope of the stress strain curve is scaled using numerical characteristic length such that the mode specific strain energy density $W_M^{(\beta\gamma)}$ and the strain energy release rate $G_M^{(\beta\gamma)}$ in mode M ($M = I$, II, or III) are related.

$$l_C^{(\beta\gamma)} W_M^{(\beta\gamma)} = G_M^{(\beta\gamma)} \tag{2}$$

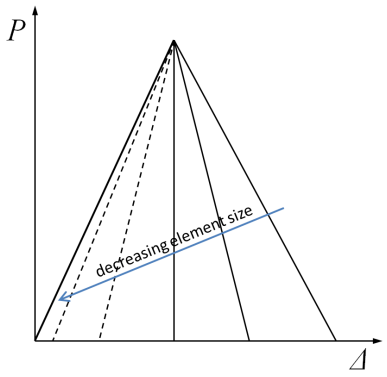

Figure 3. Effects of element size on overall load-displacement response for a material exhibiting post-peak softening. Dashed lines indicate non-physical snapback.

This scaling is enforced locally within each subcell $\beta\gamma$ (shown in Figure 1), and the characteristic length $l_C^{(\beta\gamma)}$ is calculated as the dimension of the subcell perpendicular to the crack band. Thus, the energy in the crack band is dissipated across the entire subcell. For complete details on the implementation of the crack band model in GMC (or HFGMC), the reader is referred to [9].

In order to retain mesh objectivity in a multiscale model, both the energy density and energy release rate must be preserved at, and across, all scales. Utilizing the crack band model within the GMC micromechanics ensures objectivity at the microscale. However, there must be a consistent relationship between the characteristic lengths at each scale in order to preserve the total energy release rate across the scales. In the following sections, two methods are proposed for preserving both the energy density and strain energy release rates across the scales.

Method 1: Direct Scaling

Communication between the finite element integration points and the GMC RUC is achieved through the global stress $\bar{\boldsymbol{\sigma}}$ and strain $\bar{\boldsymbol{\epsilon}}$ measures, see Figure 4. The global stress and strains are the fields at corresponding element integration points and also represent the average global stresses and strains applied to the RUC. In addition the material Jacobian, or tangent stiffness matrix, of the RUC calculated by GMC can be passed to the FEM and used to formulate the element stiffness matrix and/or estimate the next global strain increment.

The energy density can be defined at the microscale for the RUC

$$W^{RUC} = \int \bar{\sigma}_{ij}^{RUC} d\bar{\epsilon}_{ij}^{RUC} \tag{3}$$

where $\bar{\sigma}_{ij}^{RUC}$ and $\bar{\epsilon}_{ij}^{RUC}$ are the components of the global, average stress and strain tensors applied to the RUC, and the energy density can be defined at the macroscale for an integration point

$$W^{int} = \int \bar{\sigma}_{ij}^{int} d\bar{\epsilon}_{ij}^{int} \tag{4}$$

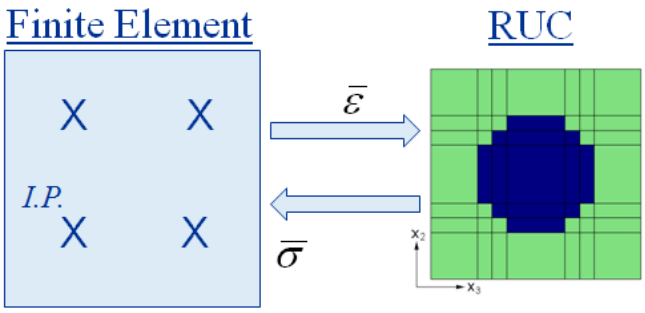

Figure 4. Schematic communication between macroscale finite element integration point and microscale GMC RUC. Global strains are passed down to the microscale and global stresses are passed back up to the macroscale.

where $\bar{\sigma}_{ij}^{int}$ and $\bar{\epsilon}_{ij}^{int}$ are the components of the stress and strain tensors at the finite element integration point.

Since, using the previously described handshaking method, the global stresses and strains are maintained across the scales (i.e., $\bar{\sigma}_{ij}^{int} = \bar{\sigma}_{ij}^{RUC}$ and $\bar{\epsilon}_{ij}^{int} = \bar{\epsilon}_{ij}^{RUC}$, it follows that the energy density is automatically preserved.

$$W^{int} = W^{RUC} \tag{5}$$

The energy density for the finite element can be taken as the volume averaged sum of the energy density of all the integration points within that finite element

$$W^{e} = \frac{1}{V^{e}} \sum_{int=1}^{nint} W^{int} V^{int} \tag{6}$$

where V^{int} and V^{e} are the integration point sub-volumes and element volume, respectively.

In addition to the energy density, the energy release rate must be preserved across the scales. The energy release rate, or fracture energy, is defined as the energy density (in the absence of plastic strain accumulation) multiplied by some characteristic length associated with the localization band [6, 18, 19, 3, 20]. Thus, the total energy release rate for the RUC at the microscale is given by

$$\mathcal{G}^{RUC} = l_C^{RUC} W^{RUC} \tag{7}$$

where l_C^{RUC} is the characteristic material length associated with strain softening in the RUC. Similarly, the energy release rate for the integration point at the macroscale is defined as

$$\mathcal{G}^{int} = l_C^{int} W^{int} \tag{8}$$

where l_C^{int} is the characteristic length associated with the integration point. It follows that the total energy release rate of the finite element is obtained from the volume averaged sum of the energy release rates of the integration points.

$$\mathcal{G}^{e} = \frac{1}{V^{e}} \sum_{int=1}^{nint} \mathcal{G}^{int} V^{int} \tag{9}$$

In order for the energy release rates at both scales to be equal, the characteristic lengths associated with the finite element integration point and the RUC must be equivalent. At the subcell level, it is trivial to define the characteristic length, $l_C^{(\beta\gamma)}$—it is simply the length of the subcell perpendicular to the crack band. However, the characteristic length of the RUC is a result of the evolution of the crack band(s) in multiple subcells contained within the RUC. Since, the crack band path is complex, and the final configuration is not known *a priori* it cannot be calculated and delivered to the macroscale to ensure that the lengths are equal.

Moreover, there is a restriction placed on the minimum allowable size of the macroscale element. The element (or integration point sub-volumes) must be large enough to contain the characteristic length of the RUC, or a suitably large RVE containing enough fibers needed to represent the localization objectively [21, 22, 9]. If the element is too small, then microscale homogenization techniques are not valid and physics is violated.

If the size and shape of the RUC and integration point sub-volume are identical, then all lengths must be consistent across the scales, automatically. This statement holds true for the characteristic lengths also, even if they cannot be calculated or defined. Unfortunately, GMC only admits rectangular RUCs (although a new isoparametric mapping technique has been developed for HFGMC [23]), and it is impractical to assume the finite element mesh will contain only rectangular elements. Particularly when modeling structural components, generally shaped quadrilaterals for 2D, or hexahedra for 3D, structures are more appropriate.

It can be assumed that the characteristic length of a 2D element integration point is equal to the square root of its area.

$$l_C^{int} = \sqrt{A^{int}} \tag{10}$$

A similar relationship can be assumed for the doubly-periodic RUC

$$l_C^{RUC} = \sqrt{A^{RUC}} \tag{11}$$

where H and L are the RUC dimensions given in Figure 1. If the dimensions H and L are scaled such that the new values (denoted by a prime symbol) are given by

$$H' = \frac{l_C^{int} H}{\sqrt{HL}} \tag{12}$$

$$L' = \frac{l_C^{int} L}{\sqrt{HL}} \tag{13}$$

then utilizing Equations (12) and (13) in Equation (11) results in equivalent characteristic lengths at both scales, that is,

$$l_C^{RUC} = l_C^{int} \tag{14}$$

Finally, substituting Equations (5) and (14) into Equations (7) and (8) yields

$$\mathcal{G}^{int} = \mathcal{G}^{RUC} \tag{15}$$

which, along with Equation (5), is a necessary condition for mesh objective multiscale modeling of strain softening behavior.

Method 2: Characteristic length mapping

As described in the previous section, all characteristic subcell lengths can be calculated correctly by scaling the dimensions of the RUC appropriately, if the shapes of the element and RUC are the same. However, this is an idealization that rarely occurs in practical multiscale analyses. Instead a transformation, similar to that used in FEM to map general quadrilaterals to a unit square[24], is utilized to map the subcell characteristic to the finite element domain.

Instead of the RUC being linked to an square finite element, as shown in Figure 4, the RUC (in the x_2-x_3 coordinate frame) is linked to a generic quadrilateral finite element (in the X-Y coordinate frame, see Figure 5. The corners of the element are represented with nodes 1, 2, 3, and 4. A reduced integration element is shown, but the same mapping technique applies except the domain the characteristic lengths are mapped to would be the integration point domain, not the entire element domain. Furthermore, the corners or the integration point domain would not necessarily all be nodes, but some points within the element domain.

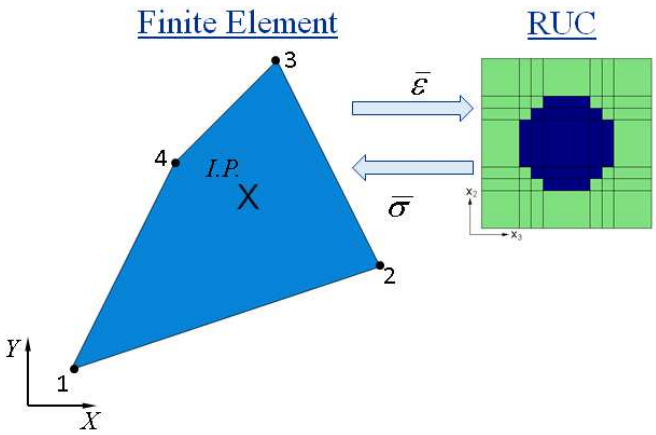

Figure 5. Schematic communication between macroscale, general quadrilateral, finite element and microscale GMC RUC. Global strains are passed down to the microscale and global stresses are passed back up to the macroscale.

A set of linear shape functions is defined for any point with coordinates x_2,

x_3 within the rectangular RUC domain.

$$\begin{aligned} N_1(x_2, x_3) &= \frac{1}{HL}(H - x_2)(L - x_3) \\ N_2(x_2, x_3) &= \frac{1}{HL} x_2 (L - x_3) \\ N_3(x_2, x_3) &= \frac{1}{HL} x_2 x_3 \\ N_4(x_2, x_3) &= \frac{1}{HL}(H - x_2) x_3 \end{aligned} \tag{16}$$

Just like with finite elements shape functions, each of the shape functions has a value of one at a unique corner and zero at every other corner in the RUC domain. The mapped position of the local x_2, x_3 point in the global domain X, Y is can be determined using the shape functions in Equation (16)

$$\begin{aligned} X &= \sum_{i=1}^{4} N_i(x_2, x_3) X_i \\ Y &= \sum_{i=1}^{4} N_i(x_2, x_3) Y_i \end{aligned} \tag{17}$$

where X_i and Y_i are the coordinates of the finite element node (or integration point domain corner) in the global frame.

Using Equations (16) and (17), characteristic subcell lengths can be mapped to the global domain. These mapped lengths are then used in the crack band theory (Equation (2) to calculate the softening slope of the stress strain curve. Figure 6 shows the characteristic length mapping process. A 7x7 RUC (shown on the left of Figure 6) is loaded in transverse tension until failure. The red lines represent the characteristic subcell lengths, which is of the subcell that is perpendicular to the crack band within that subcell. The mapped domain and mapped characteristic lengths are shown on the right of Figure 6. Note that the local fields are not calculated in the global, mapped domain; thus the local fields are not affect by distortion of the fiber in the global frame. The characteristic lengths are the only mapped dimensions that are used in the local GMC calculations, and they are only utilized within the crack band theory.

Numerical Example - Finite-notched DCB

Multiscale Model Details

To demonstrate the effects of appropriate microscale RUC length scaling, a simple multiscale example was chosen representing a modified DCB specimen. The global geometry of the modified DCB is shown in Figure 7. The total specimen length was 100 mm, with a height of 6 mm. Plane strain conditions were assumed. A 25.5 mm notch was placed at one end of the specimen. Since

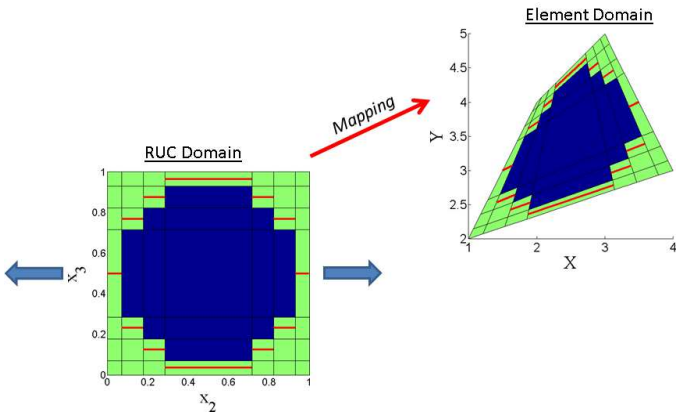

Figure 6. Mapping of characteristic subcell lengths from local, RUC domain to global finite element domain. Only mapped characteristic lengths are used in GMC calculations. The mapped fiber domain is shown only for demonstrative purposes.

Property	Value
E_{zz}	171.4 GPa
E_{xx}	9.08 GPa
ν_{zx}	0.32
G_{zx}	5.29 GPa

TABLE I. Elastic transversely isotropic properties for IM7/8552 lamina used in single scale elements[26].

continuum elements were used to model the domain and incorporate damage, a notch with a tip of a finite diameter (1 mm) was chosen so that a converged stress solution could be obtained. If a sharp crack had been chosen, the stress concentration at the notch tip could not be calculated properly. The focus of this work was to isolate mesh dependence due to post-peak strain softening. Hence, it was desirable to eliminate the dependence of the elastic solution on the global mesh size, altogether.

The entire domain was meshed using 2D, plane strain, reduced integration, quadrilateral CPE4R, and triangular CPE3 Abaqus elements [25]. A mesh sensitivity study was conducted and it was determined that using an element size l^e (see Figure 7) of 0.075 mm, or smaller, ahead of the notch tip would yield a converged, elastic, stress state at the notch tip. Figure 8 shows the coarsest mesh used in the studies incorporating a 0.075 mm by 0.075 mm elements ahead of the notch tip. Figure 8b shows a magnified view of the mesh surrounding the notch tip where the multiscale element dimensions are l_e x h_e. Assuming a fiber diameter of 5μm, an element of this size would contain nearly 170 fibers, which is adequate to justify the use of periodic boundary conditions, initially.

The macroscale domain lies in an X-Y-Z coordinate system. The model is intended to simulate matrix cracking in a 90°, IM7-8552 laminate, so the fiber direction is aligned with the global Z-axis. For simplicity, and efficiency, the majority of the elements, represented with green in Figures 7 and 8, uti-

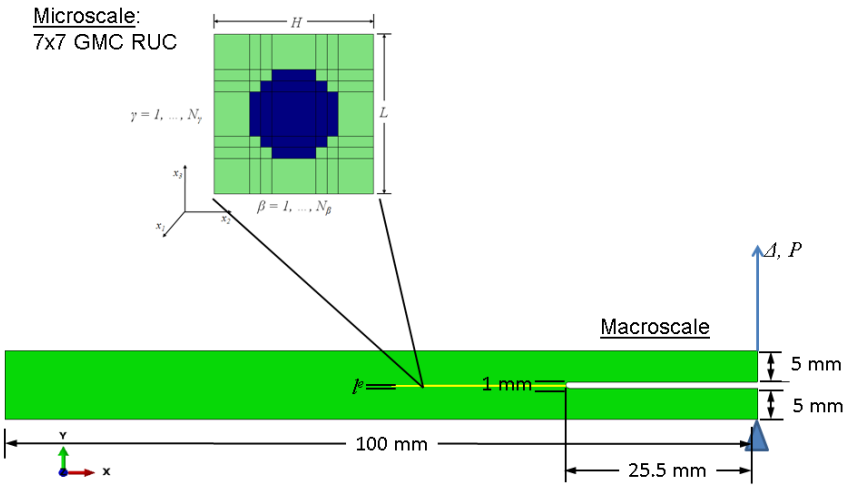

Figure 7. Multiscale model of finite-notched DCB specimen composed of a 90° laminate. The macroscale domain was modeled using traditional plane strain elements and the global X-Y-Z coordinate system. Elements within the green domain utilized a single-scale, transversely isotropic, constitutive law (z-axis represents the fiber direction). Elements within the yellow domain, ahead of the notch tip, were linked to a microscale GMC RUC. The microscale RUC consisted of a doubly-periodic, 7 subcell by 7 subcell RUC with a local x_1-x_2-x_3 coordinate system. The RUC contained 13 fiber subcells (colored blue) and 36 matrix subcells (colored green), and the local fiber direction, x_1, was aligned with the global Z-axis.

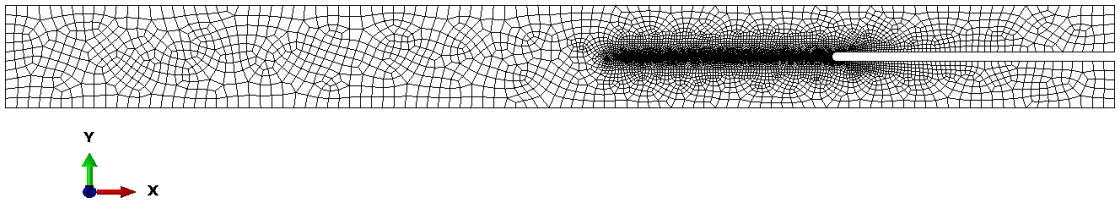

(a) Global view.

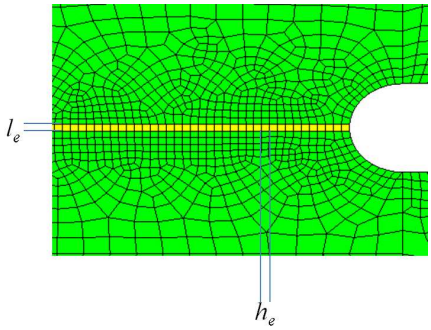

(b) Magnified view of square element mesh near notch tip.

Figure 8. FEM mesh of multiscale modified DCB.

8552 Matrix Properties	Value	IM7 Fiber Properties	Value
E^m (calibrated)	4.97 GPa	E^f_{11} (calibrated)	286 GPa
ν_m (calibrated)	0.36	E^f_{22} [27]	12.4 GPa
		ν^f_{12} (calibrated)	0.29
		ν^f_{23} (calibrated)	0.29
		G^f_{12} [27]	20.0 GPa

TABLE II. Elastic properties of IM7 carbon fiber and 8552 epoxy matrix constituents used in microscale GMC RUC.

lized a single-scale, elastic, transversely isotropic constitutive law. The elastic properties for IM7/8552 are given in Table I [26].

The elements along the expected macroscale crack path, represented in yellow, were linked to a microscale, GMC RUC using FEAMAC. The microscale model consisted of a 7 subcell by 7 subcell RUC with a local x_1-x_2-x_3 coordinate system. The RUC was composed of 13 subcells comprised of the fiber constituent (colored blue, see Figure 7) and 36 subcells comprised of the matrix constituent (colored green). A fiber volume fraction V_f of 60% was maintained. The axial, fiber direction, x_1, is aligned with the global z-axis. This choice of RUC may not be completely suitable once localization occurs, since the size of the localization typically spans one, or multiple, unit cells. An RVE containing multiple fibers is more appropriate to capture the effects of the microscale localization objectively. The intention of this work was not to offer blind failure predictions using the multiscale methodology, or to investigate solutions objectivity relative to RVE size and complexity, but rather to demonstrate the necessity for energy preservation and consistent handshaking methods across the scales. Thus, the simple and efficient RUC was chosen for its computational speed advantages and tractability, so that numerous multiscale simulations could be achieved in a reasonable amount of time. Furthermore, determining an adequate size and level of detail for the RVE, when there is localization at the subscale, remains an ongoing research area [21, 22, 9].

The elastic properties of the fiber (transversely isotropic) and matrix (isotropic) are given in Table II. These properties were calibrated such that the global RUC properties calculated using the 7 x 7 GMC RUC corresponded to the elastic properties given in Table I. The transverse fiber stiffness E^f_{22}, and axial shear modulus G^f_{12} were taken from [27].

The crack band theory was used to dictate failure in the matrix subcells. The transverse strength and mode I fracture toughness of a unidirectional, IM7/8552 ply was reported by [26] as 62.3 MPa and 0.2774 kJ/m^2. The same, single-fiber, 7 x 7 RUC was used, assuming a fiber diameter of 5 μm, to calibrate the matrix strength and fracture toughness. Using the standalone MAC/GMC micromechanics software, the RUC was loaded under transverse strain and the matrix properties were adjusted until the global RUC exhibited a strength and total energy release rate upon failure corresponded to the values reported in [26]. The resulting properties are presented in Table III.

Mode I Cohesive Strength $\sigma_C^{(\beta\gamma)}$	Mode I Fracture Toughness $\mathcal{G}_{IC}^{(\beta\gamma)}$
56.5 MPa	0.266 kJ/m^2

TABLE III. Crack band failure parameters used in 8552 matrix subcells.

The focus of this work was to determine the effects of incorporating a consistent length across the scales in a multiscale analysis. The yellow domain containing multiscale elements, shown in Figures 7 and 8, utilized fixed element shapes and sizes. Since single integration point elements were used, the characteristic length of the elements and integration point sub-volumes are identical.

$$l_C^e = l_C^{int} \tag{18}$$

The element sizes in front of the notch tip corresponding to the multiscale elements were decreased from 0.075 mm, the maximum allowable element size needed to obtain a converged stress state at the notch tip. Three types of analyses were performed: direct scaling (Scaled), characteristic subcell length mapping (Mapped), and unscaled (Unscaled). Scaled analyses utilized Equations (12) and (13) to scale the dimensions of the RUC so that they corresponded to the element dimensions. Mapped analyses utilized Equations (16) and (17) to map the characteristic subcell lengths to the element domain. Finally, Unscaled analysis assumed fixed RUC dimensions equal to 0.075 mm x 0.075 mm. When the RUC dimensions are scaled the volume of the RUC represents a physical volume, similar to an RVE. However, due to the simplicity of the fiber/matrix architecture it cannot statistically represent the heterogeneous nature of the composite and periodic boundary conditions are still utilized; thus, this scaled unit cell will still be referred to as an RUC.

Numerical Results

Figure 9 shows the error in the ultimate load predicted from the two different analysis types (Scaled and Unscaled) assuming square elements ($l_e = h_e$). Since both the shape and dimensions of the RUC (Unscaled) are identical for the 0.075 mm element case it is assumed to be the most correct solution. All error in the ultimate load is calculated in the other analyses using the 0.075 mm results as the baseline. Note that the Mapped analyses were not included in this figure because for an element with an aspect ratio of one the results are identical to the Scaled analyses. The element size was varied from 0.075 mm to 0.045 mm (which could still accommodate 61 fibers at a 60% fiber volume fraction) in increments of 0.05 mm. Filled markers signify that the RUC dimensions were scaled according to the assumed characteristic element length (Equation (10)) using Equations (12) and (13), and open markers denote that a fixed RUC size of 0.075mm x 0.075mm was used.

When square elements with scaled RUCs were used, the ultimate load predicted during the simulations remained within 1% of the baseline. Whereas, not performing the scaling appropriately led to a steady reduction in the ultimate

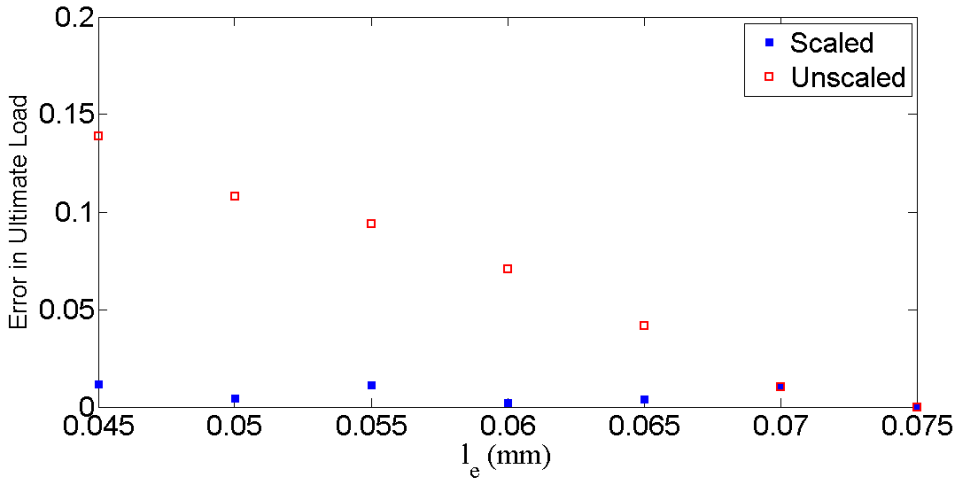

Figure 9. Error in ultimate load predicted with multiscale, modified DCB simulations incorporating square elements along the crack path. Results compared for microscale RUC scaled by element length to fixed RUC dimensions of 0.075 mm x 0.075 mm.

load as the element size was decreased. Using a square element with length 0.045 mm, and an unscaled RUC, yielded an ultimate load prediction of 14% error from the baseline analyses. This pathological mesh dependence is the most significant limitation of multiscale modeling identified by [15], as it yields inconsistent and unreliable predictions. However, as shown, with the appropriate "handshaking" methodology and the use mesh independent damage theories at the microscale, this pathological dependence on the discretization size can be eliminated at all scales.

However, the results in Figure 9 utilize square element, which are not practical for most engineering analyses. To interrogate the robustness of the scaling technique and evaluate the effectiveness of the mapping technique (results not shown yet), analyses are performed with rectangular elements of varying aspect ratio. The X-dimension h_e of the elements are fixed at 0.075 mm, and the Y-dimensions l_e are varied from 0.07 mm to 0.045 mm. Figure 10 shows the error in ultimate load (compared to baseline 0.075 mm x 0.075 mm square element results) as a function of element height l_e for Mapped, Scaled, and Unscaled characteristic subcell lengths. The Mapped and Scaled techniques yield more accurate ultimate load predictions than performing no adjustment to the local subcell characteristic lengths (Unscaled). However, their is still some error introduced and it seems to be increasing pathologically as the aspect ratio of the element deviates from one.

Figure 11 shows the actual ultimate load versus element height for the three different length scale "handshaking" methods. It can be seen that the predicted ultimate load decreases as function of element height when the Scaled technique is used, but increases when the Mapped technique is used. This indicates that the Scaled technique is overestimating the characteristic length of the RUC, while the Mapped technique is underestimating it.

The maximum error in the Unscaled results was improved from 13.8 % to 6.5

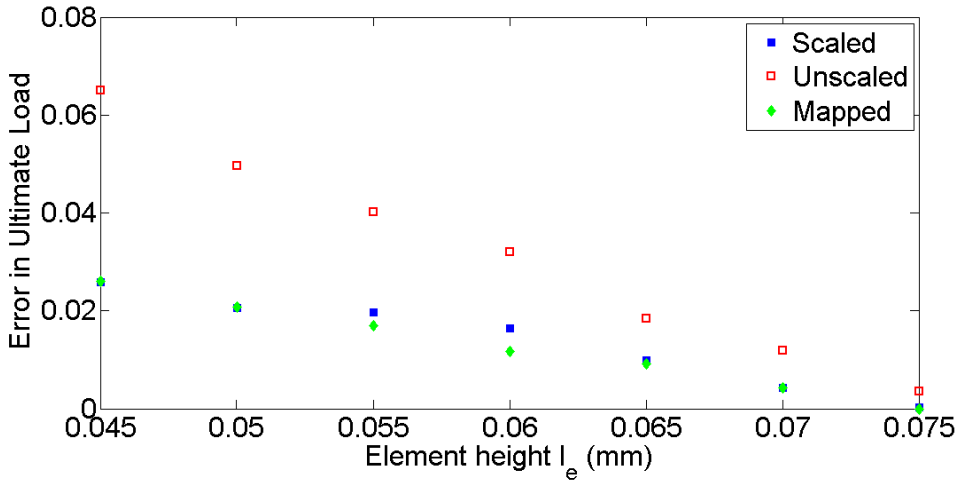

Figure 10. Error in ultimate load predicted with multiscale, modified DCB simulations incorporating rectangular elements along the crack path. Element length l_e, and thus aspect ratio, was varied while element height was fixed at 0.075 mm.

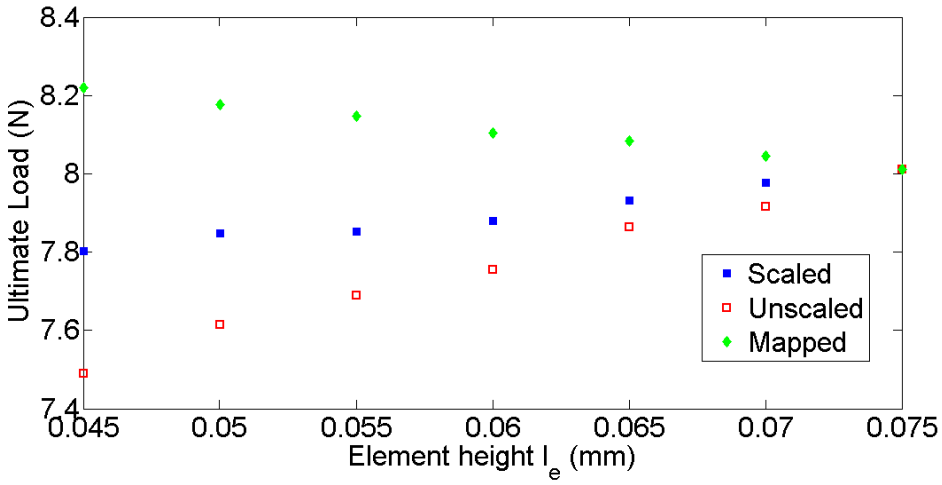

Figure 11. Ultimate load predicted with multiscale, modified DCB simulations incorporating rectangular elements along the crack path. Element length l_e, and thus aspect ratio, was varied while element height was fixed at 0.075 mm.

% with the rectangular elements (Figure 10) over the square elements (Figure 9). With the rectangular elements the length of the RUC h_e and element are still the same (0.075 mm). This implies that both the RUC length and height (relative to the element) influence the amount of energy dissipated even though the global crack path is always normal to the global Y direction.

As a result, further investigations are required to determine how to effectively scale the local subcell characteristic lengths such that the characteristic length of the RUC and the element (or integration point) volume are coincident. This is a challenging task because the characteristic length of the RUC cannot be determined, and as such cannot be scaled, *a priori*. It is a function of how much energy is released during local softening damage evolution. Thus, it is depends on the local crack band path in the RUC and is problem dependent.

It should be noted that an unusual default RUC size and was chosen such that the RUC dimensions would match exactly with the element size used in the coarsest mesh that provided a converged, elastic stress solution. Typically, the size of an RUC is neglected in a multiscale analysis because the RUC represents an infinite number of repeating cells, due to the imposed periodic boundary conditions, and the RUC is essentially "dimensionless." Therefore, a 1 x 1 size is often used for a square RUC. When there is local strain softening, the dimensions become important. In this case, it is logical to choose the RUC dimension based on the fiber diameter, which is on the order of 0.005 mm for carbon fibers.

The maximum error using all three methods (Scaled, Unscaled, and Mapped) is relatively low (1% – 14%). However, the maximum error in the Unscaled results are a facet of the baseline RUC size that was chosen (0.075 mm x 0.075 mm). It can be expected that using more traditional RUC dimensions (on the order of 1 mm or 0.005 mm) would result in a significant increase in error. Therefore, the baseline results utilizing a 0.075 mm x 0.075 mm RUC are, in essence, results utilizing a "Scaled" approach. So, although there is still error introduced with the Scaled or Mapped techniques when the element is not square, this error is limited to a few percent and is a vast improvement over what would be expected if no attention is given to the size of the RUC, and "typical" RUC dimensions are used.

Conclusions

To accurately predict the failure of a material with a numerical model local strain softening must be modeled and must be insensitive to changes in the finite element mesh. To achieve this mesh objectivity the local energy density dissipation can be scaled, or regularized, using a characteristic length such that the energy release rate. Multiscale modeling is a popular technique used to model composite materials, or other materials where the microstructure influences the behavior of the structure. However, when performing a multiscale analysis, it is necessary to ensure that the energy dissipation is regularized appropriately at both scales, or preserved across the scales with the chosen handshaking method.

With FEAMAC (a multiscale analysis tool that links the GMC micromechanics theory to FEM), information is transmitted across the scales through the global (or finite element integration point) stress and strain tensors. This handshaking method does not ensure that the energy dissipation is preserved across the scales and will yield pathological mesh dependence when there is failure. In an attempt to regularize the energy dissipation at the microscale appropriately, two techniques were developed. With the first technique, the dimensions of the microscale RUC are scaled such that they coincide with the square root of the area of the element. Using this scaling technique, pathological mesh dependence was eliminated for square elements.

However, practical finite element models utilize elements which are not square. Therefore, a second technique was developed which mapped the local characteristic lengths of the subcells to the macroscale. The mapped characteristic lengths were then used in the subcell crack band calculations to regularize the energy dissipated in the subcells. Unfortunately, neither technique (scaling or mapping) eliminated the mesh dependence when rectangular elements were used. However, the error is was minimized to less than a maximum of 3% for an element with an aspect ratio of 0.6.

The resulting error indicates that the two techniques are not accurately predicting the characteristic length of the RUC. This is a major challenge in multiscale analysis because the characteristic length of the RUC is not fixed, but rather depends on the energy dissipated locally due to strain softening and the local crack path. Thus, it depends on the multi-axial stress state of the element and is problem dependent. Future work will focus on improving the techniques used to determine the characteristic length of the RUC.

REFERENCES

1. Sullivan, R. W. and Arnold, S. M. 2011. In S. M. Arnold and T. T. Wong, (ed.), Models, Databases, and Simulation Tools Needed for the Realization of Integrated Computational Materials Engineering: Proceedings of the Symposium Held at Materials Science & Technology 2010, Houston, Texas: ASM International. pp. 6–23.
2. Aboudi, J., Arnold, S. M., and Bednarcyk, B. A. 2013. Micromechanics of Composite Materials: A Generalized Multiscale Analysis Approach, Elsevier, Inc., .
3. Bažant, Z. P. and Cedolin, L. 1991. Stability of Structures: Elastic, Inelastic, Fracture and Damage Theories, Oxford University Press, New York, Oxford, .
4. Bažant, Z. and Cedolin, L. 1979. "Blunt crack band propagation in finite element analysis," *J. Eng. Mech. Div.-ASCE* **105**, 297–315.
5. Pietruszczak, S. and Mroz, Z. 1981. "Finite element analysis of deformation of strain-softening materials," *Int. J. Numer. Methods Eng.* **17**, 327–334.
6. Bažant, Z. P. and Oh, B. H. 1983. "Crack band theory for fracture of concrete," *Mater. and Struct.* **16**, 155–77.
7. deBorst, R. and Nauta, P. 1985. "Non-orthogonal cracks in a smeared finite element model," *Eng. Comput.* **2**, 35–46.
8. Rots, J. G. and deBorst, R. 1987. "Analysis of mixed-mode fracture in concrete," *J. Eng. Mech.* **113(11)**, 1739–1758.
9. Pineda, E. J., Bednarcyk, B. A., Waas, A. M., and Arnold, S. M. 2013. "Progressive failure of a unidirectional fiber-reinforced composite using the method of cells: Discretization objective computational results," *Int. J. Solids Struct.* **50(9)**, 1203–1216.

10. Paley, M. and Aboudi, J. 1992. "Micromechanical Analysis of Composites by the Generalized Cells Model," *Mechanics of Materials* **14**, 127–139.
11. Aboudi, J., Pindera, M.-J., and Arnold, S. M. 2001. "Linear thermoelastic higher-order theory for periodic multiphase materials," *J. Appl. Mech.* **68**, 697–707.
12. Eringen, A. C. 1966. "A unified theory of thermomechanical materials," *Int. J. Eng. Sci.* **4**, 179–202.
13. Bažant, Z. P. 1994. "Nonlocal damage theory based on micromechanics of crack interactions," *J. Eng. Mech. - ASCE* **120(3)**, 593–617.
14. Jirásek, M. 1998. "Nonlocal models for damage and fracture: Comparision of approaches," *Int. J. Solids Struct.* **35(31-32)**, 4133–4145.
15. Bažant, Z. P. 2007. "Can multiscale-multiphysics methods predict softening damage and structural failure?," *Mech. Amer. Acad. Mech.* **36(5-6)**, 5–12.
16. Pineda, E. J., Bednarcyk, B. A., Waas, A. M., and Arnold, S. M. 2013. "On multiscale modeling using the generalized method of cells: Preserving energy dissipation across disparate length scales," *CMC-Comput. Mater. Con.* **25(2)**, 119–154.
17. deBorst, R. 1987. "Computation of post-bifurcation and post-failure behavior of strain-softening solids," *Comput. Struct.* **25**, 211–224.
18. Rots, J. G., Nauta, P., Kusters, G. M. A., and Blaauwendraad, J. 1985. "Smeared crack approach and fracture localization in concrete," *HERON* **30(1)**, 1–48.
19. Oliver, J. 1989. "A consistent characteristic length for smeared cracking models," *Int. J. Numer. Meth. Eng.* **28**, 461–474.
20. Bažant, Z. P. 2005. Scaling of Stuctural Strength, Elsevier, Ltd., second edition.
21. Totry, E., Gonzaléz, C., and Llorca, J. 2008. "Influence of the loading path on the strength of fiber-reinforced composites subjected to transverse compression and shear," *Int. J. Solids Structures* **45**, 1663–1675.
22. Heinrich, C., Aldridge, M., Wineman, A. S., Kieffer, J., Waas, A. M., and Shahwan, K. W. 2013. "The Role of Curing Stresses in Subsequent Response, Damage and Failure of Textile Polymer Composites," *J. Mech. Phys. Solids* **61**, 1241–1264.
23. Haj-Ali, R. and Aboudi, J. 2013. "A new and general formulation of the parametric HFGMC micromechanical method for two and three-dimensional multi-phase composites," *Int. J. Solids Struct.* **50**, 907–919.
24. Hughes, T. J. R. 2000. The Finite Element Method: Linear Static and Dynamic Finite Element Analysis, Dover Publications, Inc., Mineola, New York.
25. Dassault Systèmes Simulia Corp. Abaqus User's Manual, Vol. 1-3, Version 6.11-1 Dassault Systèmes Simulia Corp. Providence, RI 2011.
26. Camanho, P. P., Maimí, P., and Dávila, C. G. 2007. "Prediction of size effects in notched laminates using continuum damage mechanics," *Compos. Sci. and Technol.* **67**, 2715–2727.
27. Goldberg, R. K. and Gilat, A. 2003. In C. E. Bakis, (ed.), Composite Material: Testing and Design Fourteenth Volume, ASTMSTP 1436, : ASTM International, West Conshohocken, PA.